Drainage and erosion of Cambodia's Great Lake in the middle-late Holocene: the combined role of climatic drying, base-level fall and river capture

Stephen E. Darby[1], Peter G. Langdon[1], James L. Best[2,3], Julian Leyland[1], Christopher R. Hackney[4], Mackenzie Marti[2*], Peter R. Morgan[1], Savuth Ben[5], Rolf Aalto[6], Daniel R. Parsons[7], Andrew P. Nicholas[6] and Melanie J. Leng[8]

[1]School of Geography and Environmental Science, University of Southampton, Highfield, Southampton, SO17 1BJ, UK

[2]Department of Geology, University of Illinois at Urbana-Champaign, Urbana, IL 61801, USA

[3]Departments of Geography and GIS, Mechanical Science and Engineering and Ven Te Chow Hydrosystems Laboratory, University of Illinois at Urbana-Champaign, Urbana, IL 61801, USA

[4]School of Geography, Politics and Sociology, University of Newcastle, Newcastle-Upon-Tyne, NE1 7RD

[5]Ministry of Mines and Energy, 79-89 Pasteur Street, Sangkat Phsar Thmey, Khan Daun Penh, Phnom Penh, Cambodia

[6]Department of Geography, University of Exeter, Exeter, EX4 4RJ, UK

[7]Energy and Environment Institute, University of Hull, Hull, HU6 7RX, UK

[8]British Geological Survey, Keyworth, Nottingham NG12 5GG, UK and Centre for Environmental Geochemistry, School of Biosciences, University of Nottingham, LE12 5RD

**now at: Illinois State Geological Survey, Prairie Research Institute, Champaign, IL 61820, USA*

Corresponding Author: Stephen E. Darby (S.E.Darby@soton.ac.uk)

ABSTRACT

We provide evidence for a large-scale geomorphic event in Cambodia's great lake, the Tonlé Sap, during the middle Holocene. The present-day hydrology of the basin is dominated by an annual flood pulse where water from the Mekong River raises the lake level by *c.* 8m during the monsoon season. We present new subsurface geophysical data, allied to new and past core studies, which unequivocally show a period of major mid-Holocene erosion across the entire Tonlé Sap basin that is coincident with establishment of the lake's flood pulse. We argue that this widespread erosion, which removed at least 1.2 m of sediment across the lake's extent, was triggered by up to three, likely interacting, processes: (1) base-level lowering due to mid-Holocene sea-level fall, leading to (2) capture of the Tonlé Sap drainage by the Mekong River, and (3) a drying climate that also reduced lake level. Longer-term landscape evolution was thus punctuated by a rapid, river capture- and base-level fall-induced, lake drainage that established the ecosystem that flourishes today. The scale of change induced by this mid-Holocene river capture event demonstrates the susceptibility of the Tonlé Sap to ongoing changes in local base-level and hydrology induced by anthropogenic activity, such as damming and sand mining, within the Mekong River Basin.

Keywords: Tonlé Sap, Holocene; Paleogeography; Paleolimnology; Southeastern Asia

1. INTRODUCTION

Draining the Tibetan Plateau and the Annamite Mountains bordering Laos and Vietnam, the Mekong River is an iconic but threatened river system. Not only is the Mekong one of the world's largest rivers, generating large fluxes of water (450 km^3 yr^{-1}; MRC, 2005) and sediment (~87 Mt yr^{-1}; Darby *et al*., 2016), it is (after the Amazon) the second most biodiverse river on the planet (Ziv *et al*., 2012).

Critical in supporting and sustaining the Mekong's rich ecosystem is Cambodia's great lake, the Tonlé Sap. The Tonlé Sap Lake lies within a sub-catchment (drainage area of 85,790 km^2, around 11% of the total area) of the Mekong and forms the largest freshwater body in southeast Asia (measuring *c.* 2,400 km^2 during the dry season but expanding to *c.* 10,800 km^2 during the rainy season; Kummu and Sarkkula, 2008). The defining feature of the lake is its remarkable hydrology, whereby the Tonlé Sap River exhibits a seasonal reversal of its flow direction. In the dry season (November to April), the Tonlé Sap drains under gravity to the Mekong River at the Chaktomuk confluence at Phnom Penh (Figure 1). In the wet season, from May to October, the Mekong's water levels rise higher than those in the Tonlé Sap, inducing a pressure gradient that causes the Tonlé Sap River to reverse direction and flow back towards the Tonlé Sap Lake. Similar to other seasonally flooded systems (Junk *et al*., 1989; Junk *et al*., 1997a, b), this annual flood pulse drives exceptionally high ecological productivity (Rainboth, 1996; Sverdrup-Jensen, 2002; Junk *et al*., 2006; Lamberts, 2006; Arias *et al*., 2012). For example, the lake's fishery and associated aquaculture provide up to 80% of the protein consumption for the whole of Cambodia (Ahmed *et al*., 1998; Hortle, 2007). The ingress of Mekong flood waters during the monsoon season means that the volume of fresh water stored in the lake varies on average from 1.8 km^3 during the driest month to 58.3 km^3 during the peak flow (Kummu and Sarkkula, 2008). The Tonlé Sap lake therefore acts as a natural flood storage capacitor, storing very large volumes of flood water in the wet season, thereby significantly attenuating flood levels in the Mekong delta downstream (Kite, 2001; Hung *et al*., 2012; Piman *et al*; 2013). Conversely, the stored floodwater is released back to the Mekong River during the dry season, a key stage of the agricultural growing season, at which time approximately half of the river discharge to the Mekong Delta in Vietnam originates from the lake (Fuji *et al*., 2003; Kummu *et al*., 2014).

It is evident that the connection of the Mekong and Tonlé Sap rivers at the Chaktomuk Junction represents a critical node in the drainage network of the Mekong Basin. In recent years, knowledge of the hydrology of the Tonlé Sap system and its hydrodynamic relationship with the Mekong River mainstem has increased substantially (Fuji *et al*., 2003; Inomata and Fukami, 2008; Kummu and Sarkkula, 2008). Nevertheless, significant gaps remain, most particularly in terms of understanding the extent to which the connection, and its hydrological functioning, may be vulnerable to system responses induced by climate change and the ongoing, rapid, socio-economic development of the Mekong Basin (e.g. Arias *et al*., 2013, 2014; Kummu *et al*., 2010; Lamberts, 2008; Lamberts and Koponen, 2008; ICEM, 2010; MRC, 2018).

In part, a clear understanding of the vulnerability of the Chaktomuk connection has remained elusive because hitherto there has been no clear consensus from prior palaeo-environmental analyses regarding the timing at, and hydro-geomorphic conditions under, which the connection between the Mekong and Tonlé Sap rivers was established initially. On the one hand, distinctive changes in lithological characteristics of the two main sediment facies deposited within the lake are interpreted as representing a transition from a non-pulsing to a flood-pulsed system. Specifically, sediments below the transition only contain kaolinite and smectite clay minerals, whereas illite and chlorite are also present above the transition, which was dated in two cores to 5,081±86 ^{14}C years BP (5,615-5,992 cal. years BP) and 5,620±120 ^{14}C years BP (6,184-6,715 cal. years BP) (Okawara and Tsukawaki, 2002). Since illite and chlorite minerals are not sourced within the Tonlé Sap catchment, but rather are products of weathering in the Mekong River basin upstream, their presence is a signal of the onset of a connection between the Tonlé Sap lake and Mekong River (Okawara and Tsukawaki, 2002; Day *et al*., 2011). A more recent study (Day *et al*., 2011) has independently identified the transition from a non-connected to Mekong-connected system as being marked by shifts (dated between 4,450 and 3,910-4,450 cal. years BP) in Sr, Nd and Pb isotopes and elemental concentrations to values characteristic of modern Mekong River sediments (Day *et al*., 2011). A subsequent study by Fukumoto (2014) also argues for a Mekong connection dated to around 3,900 cal. years BP, based on evidence from a lake sediment core that shows a rise in magnetic susceptibility and some elements (notably K) around this time. Conversely, a lake sediment core collected by Penny (2006), in which mangrove pollen and diatoms tolerant of brackish conditions were found to be present in the early Holocene, was interpreted as indicating that a connection between the Tonlé Sap lake and South China Sea, via the Mekong River, has existed throughout the Holocene (Penny, 2006). These divergences in interpretations of timing, when combined with the point that the previous cores have been interpreted in isolation, without understanding their spatial context, make it challenging to clearly identify the environmental conditions during the onset and early evolution of the (postulated) connection between the Tonlé Sap Lake and the main Mekong River system.

The present paper aims to use a combination of detailed geophysical surveys and analysis of proxy records preserved in lake sediment cores, to provide new insight into the Holocene evolution of the Tonlé Sap Lake and thereby cast new light on the issues discussed above. Our findings show that the connection between the lake and the Mekong River, caused by the Mekong capturing the Tonlé Sap River, induced catastrophic (lake-wide) changes in lake drainage, causing erosion of *c.* 10 km^3 of sediment. We interpret the period of the capture (postdating ~6,200 cal. years BP) to be contemporaneous with a period of drying and declining sea-level, which would have enabled a lowering of base level and wave reworking that led to this large pulse of erosion. Our work highlights the vulnerability of the Chaktomuk connection to changes in hydro-climatic conditions, underscoring the importance of maintaining natural river flow dynamics at the Chaktomuk connection to support the Tonlé Sap Lake’s unique and highly valuable ecosystem function.

2. METHODS

We undertook geophysical surveys and analysis of lake sediment records to provide a new perspective on the palaeo-environmental history of the Tonlé Sap Lake. Specifically, we collected a new sediment core, from which geochemical and other proxy records were determined and analysed (see below for discussion of core collection and analysis, including the establishment of a chronology via radiocarbon dating and age-depth modelling) to reconstruct changing environmental conditions. As discussed fully below, we also collected over 500 km of new geophysical data (Parametric Echo Sounding; PES) survey lines, including targeting the site of our new core record as well as the sites of existing core records from prior studies (Figure 1). These PES lines provide a clear picture of the sub-bottom sediments from across the lake and hence link the new and existing published core records into a common stratigraphic framework. These new geophysical data not only provide a longer-term perspective on landscape change, but also afford the opportunity to reappraise our new and prior core sediment records within a broader stratigraphic spatial context. The clear stratigraphic correlation delivered by the geophysical data also allows for much stronger chronological control due to the ability to pool the radiocarbon dates obtained from the multiple, previously isolated, core records.

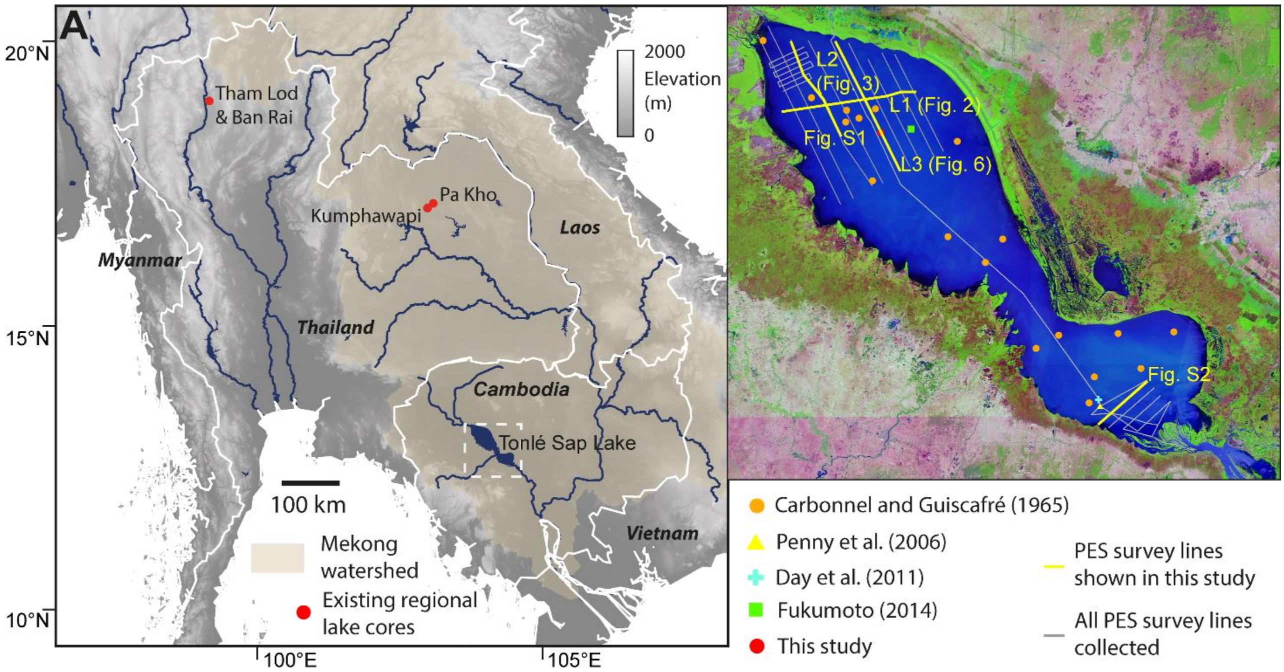

Figure 1: Location of the Tonlé Sap Lake in central Cambodia. (A) Regional context showing the Mekong catchment and locations of other regional studies of lake sediment records discussed herein (see Figure 7 in Section 4 for details), at lakes Pa Kho, Kumphawapi, Tham Lod and Ban Ra in Thailand. (B) Locations of Parametric Echo Sounding (PES) survey lines (grey lines show all PES lines collected, yellow lines identify lines shown in other diagrams; ; note that Fig. S1 and Fig. S2 are in the Supplementary Data) and new sediment core record (red circle) used in this study. The locations of previous sediment core records from the Tonlé Sap Lake and discussed in the text are also indicated.

2.1 Parametric Echo-Sounding (PES)

The sub-bottom profiling data were obtained using an Innomar SES-2000 Light Parametric Echo Sounder (PES) on October 23rd - 29th 2014, deployed from a wooden boat, providing a total of *c*. 530 km of PES transects (Figure 1). The PES was linked to an EdgeTech motion reference unit to remove any effects of vessel heave, pitch and roll, although weather conditions during the surveys were excellent, with position being given by a Leica System 1230 GPS. The PES operates by transmitting two signals of different frequency (100 kHz and a selectable lower frequency between 4 kHz and 15 kHz) that, due to the non-linearities in sound propagation at high pressures, interact and produce new acoustic frequencies (Sambrook Smith *et al*., 2013). The high-frequency signal and narrow beam footprint provide an accurate estimate of water depth, whilst the lower frequencies penetrate the bed and produce reflections from differences in sedimentary bedding/structures in the subsurface. In this manner, PES can produce high-resolution imaging of the bed topography and subsurface structure simultaneously, and its performance is particularly good in finer-grained sediments such as silts and clays. Further details of the PES are given in Sambrook Smith *et al*. (2013, 2016).

During the survey set-up, initial optimisation tests showed that a secondary frequency of 8 kHz provided the best results in terms of resolution and depth of penetration into the subsurface. The depth of water within the Tonlé Sap lake at the time of the survey was *c*. 7m, and it was found that the combination of the sediment size (median grain size *c*. 6 microns), soft lakebed sediments (that minimised a hard surface acoustic return) and the PES input power and frequencies used, often enabled imaging of reflections below the first return multiple. Thus in many, but not all, places the PES imaged strong reflections at depths up to 15 m below the lake-bed. Poor acoustic penetration was present in some areas due to subaqueous vegetation growing on the lake-bed near the shore, vegetation debris accumulated on the PES transducer, and occasional cavitation around the transducer head at higher boat speeds. However, despite these restrictions, the PES provided imaging of the subsurface with a vertical resolution of *c*. 0.15 m.

As shown in Figure 1, the PES surveys focused on ten NW-SE lines in the north of the lake, linked by one W-E line (Line 1, indicated as L1 in Figure 1), together with a smaller grid of lines at the NW of the lake. One long line was run down the centre of the entire lake, and a small grid of survey lines was collected near the delta at the southern end of the lake. Lines were also run to intersect the location of the core taken as part of this research (Core LC2; see Section 2.2), as well as a previous core taken by Day *et al*. (2011; Core TS-18-XII-03), for which detailed geochemical data are available. The co-location of the PES and core records is advantageous because it enables further ground-truthing of the PES reflections from the core records, as well as further contextualisation of the palaeo-environmental interpretations derived from the prior work. In this regard, it may also be noted that two PES lines also ran either side of, and within *c.* 1.3 km of the CT10 core site reported by Fukumoto (2014) and several of the PES lines were located close to some of the cores described by Carbonnel and Guiscafré (1965). Although the Carbonnel and Guiscafré (1965) cores are described in less detail than the more recent studies, they still provide useful further context for the PES data. A PES survey line was also run over the locality of core S2C1 from Penny (2006), although later examination of this data showed that the core location was likely in error to the level of accuracy required to geo-locate the PES results with the core characteristics. The PES-core correlation with the S2C1 core of Penny (2006) could thus not be undertaken.

The data were collected using Innomar PES software, whilst boat tracks and navigation were recorded on a separate PC running Global Mapper software. PES processing was accomplished using Innomar ISE post-processing software (Innomar, 2016) and involved accumulation of track points at a 0.2 m spacing to yield a consistently scaled horizontal distance, filtering to enhance reflections and reduce water column noise, application of a moderate time-varying gain and a smoothing using between 2 and 3 ensembles. This processing methodology yielded PES panels for all lines, and these were then used within Innomar ISE software to manually trace key surfaces that could be exported and used to estimate water depths and thicknesses of sediment packages.

2.2 Sediment Core Retrieval and Analysis

A sequence of overlapping cores was obtained from a part of the lake from which test sampling revealed to be a relatively deep infill. Coring took place in March 2013 when lake water depth was relatively low, *c*. 1.5m. A 0.6 m long core tube was used in a UWITEC gravity-type corer with core catcher to sample the upper (most recent) sediments, including the undisturbed sediment-water interface. Zorbitrol™ was used to solidify the overlying 0.05 m of water to maintain the integrity of the sediment surface, and the core was extruded and subsampled in 0.01 m sections. A 1 m-long 7 cm diameter Livingstone Piston corer was deployed to retrieve overlapping cores to a total sediment depth of 4.58 m. Upon extrusion in the field, all cores were carefully wrapped in cling film and kept in cool storage (+4 °C) until they could be sub-sampled.

The core sequences were extruded in the field and cleaned. A 0.01 m deep U-channel was taken from each core sequence and carefully wrapped. Following the U-channel sampling, the remainder of the cores were sub-sampled in the field and chopped into 0.01 m resolution contiguous slices. The individual sub-samples were analysed at the University of Southampton for loss-on-ignition (LOI) and particle size, the latter using a Micromeritics® Saturn DigiSizer® II particle size analyser. The overlapping cores were correlated using the LOI and Itrax (see below) data, with core depths then re-mapped onto a single depth model that was used for subsequent age/depth modelling. Geochemical analysis was undertaken on the U-channels using an Itrax core scanner (Cox Analytical Systems, Goethenburg, Sweden) at the National Oceanography Centre, University of Southampton. Both a photographic and X-radiographic image were obtained at high resolution prior to each core's XRF scan. The chosen resolution of the XRF scans was determined by visual inspection of the core stratigraphy for fine laminae. A Molybdenum tube (30kV, 30mA) was used to scan each core at 500 µm resolution and at 200 µm for the surface gravity core. Exposure time was set at 30 seconds.

For the organic matter geochemistry, undertaken at contiguous 0.01 m samples, $^{13}C/^{12}C$ analyses were performed by combustion in a Costech ECS4010 Elemental Analyser (EA) on-line to a VG TripleTrap and Optima dual-inlet mass spectrometer, with $\delta^{13}C$ values calculated to the VPDB scale using a within-run laboratory standards calibrated against NBS18, NBS-19 and NBS-22. Replicate analysis of well-mixed samples indicated a precision of ± <0.1‰ (1 SD). C/N ratios (including %C measurements) were calibrated against a Broccoli standard (BROC2). Replicate analysis of well-mixed samples indicated a precision of ± <0.1.

2.3 Radiocarbon dating and age-depth modelling

We used ^{14}C dating to establish a chronology for our Tonlé Sap lake core sequence. No terrestrial macrofossils were found in the sequence, only some wood fragments, requiring that most ^{14}C measurements were sourced from bulk sediment. Eleven samples were sent to Beta Analytic and prepared for ^{14}C dating using their standard methods. All eleven radiocarbon dates were used in the BACON 2.2 Bayesian modelling software (Blaauw and Christen, 2011) to create an age/depth model.

3. RESULTS AND INTERPRETATION

3.1 Overview of PES Facies

The PES imaging revealed a complex, but nevertheless consistent, series of reflectors (Table 1; Figures 2 and 3) that were classified into facies according to their principal reflection characteristics. Note that these detailed classifications provide the basis for interpretations of depositional processes and stratigraphy across the Tonlé Sap Lake and comparison (Section 3.4) with previous research. The PES profiles show four major facies based on the reflection characteristics (Table 1), revealing the presence of a palaeo-valley network across the entire Tonlé Sap lake that has been infilled by Holocene sediments (Table 1; Figures 2 and 3; also see Supplementary Data Figures S1 and S2). A strong undular basal reflector (Facies 1; Table 1; labelled ‘1’ in Figures 2 and 3; also see Supplementary Data Figures S1 and S2) is interpreted as representing the erosive surface of a likely Pleistocene valley network, with valleys up to *c*. 15 m deep, likely eroded during the sea-level low stand that accompanied the Last Glacial Maximum (Tjallingii *et al*., 2010; Fukumoto, 2014). This valley surface is overlain by sediments that have infilled the valley network and represent: i) a series of minor fluvial or valley-slope deposits (Facies 2; Table 1; labelled '2' in Figures 2 and 3; as well as Figures S1 and S2) that drape against the underlying valley sides in places, and ii) parallel-bedded lacustrine deposits that comprise the majority of the infill (Table 1; Facies 3 and 4; labelled '3a-c' and '4' in Figure 3B). The lacustrine deposits of Facies 3 are characterised by parallel, reflectors that mirror any underlying basal topography but with no internal truncations, that attest to the spatially continuous sedimentation that gradually infilled the pre-existing topography. The presence of a clear disconformity between Facies 3 and 4 (Figures 2 and 3; labelled 'e'; see also Figures S1 and S2) is indicative of an erosion surface (indicated also by radiocarbon dating, as discussed further in Section 3.3) that is present between the lacustrine Facies 3 and 4. Indeed, the disconformity can be traced across the entire Tonlé Sap lake, with the facies above this surface characterised by parallel-bedded sediments that contain individual point reflectors (Table 1; labelled 'p' in Figures 2 and 3B). These point reflectors likely represent siderite concretions (Pottier *et al*., 2012) or accumulations of the Asiatic clam *Corbicula fluminaea* (Penny, 2006) that are commonly found in the upper layer of the Tonlé Sap lake sediments. If the thickness of the parallel reflectors in Facies 3 that are truncated by the erosion surface are examined (Figure 2, inset X), it is evident that erosion of *c*. 1.2 m of lacustrine sediment must have taken place before the resumption of lacustrine sedimentation in Facies 4, a key point that is returned to below. However, the amplitude of relief along this erosional surface is small, with one N-S transect line in the north of the Tonlé Sap lake (location marked L3 on Figure 1) showing an erosional relief of 0.85 m along a transect length of 10 km. Overall, the new PES data thus show the occurrence of a major episode of lake-bed erosion that very likely extends across the entire lake (the disconformity being expressed across the entire 530 km extent of our PES survey), producing the disconformity between Facies 3 and 4.

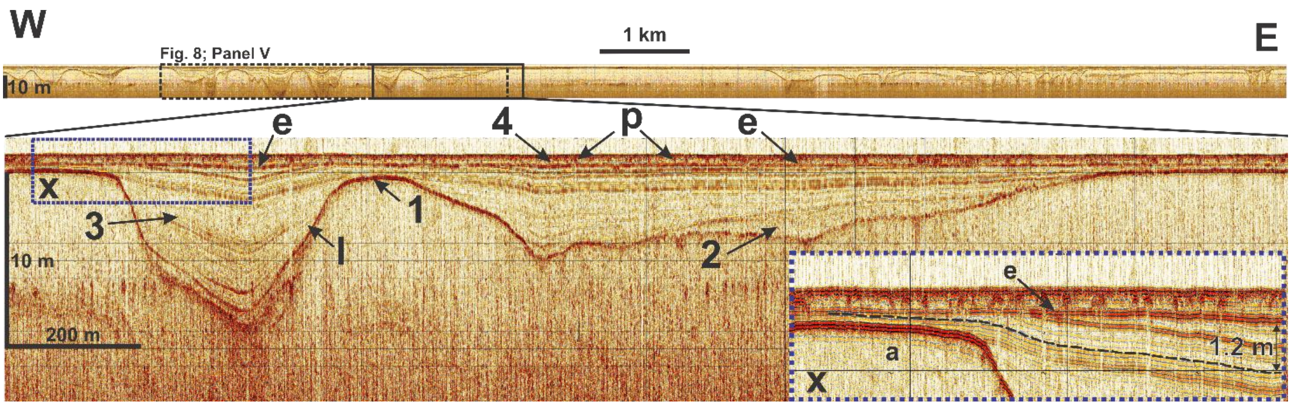

Figure 2: PES profiles of Line 1 (see L1 on Figure 1 for location) running W-E across the Tonlé Sap Lake, illustrating the principal palaeo-valleys and PES Facies 1-4, with the labels being detailed in the text and Table 1. Top profile is 14.25 km wide, with area in black rectangle shown in detail below. Inset X illustrates the truncation of reflectors used to estimate the amount of erosion at *c.* 1.2m.

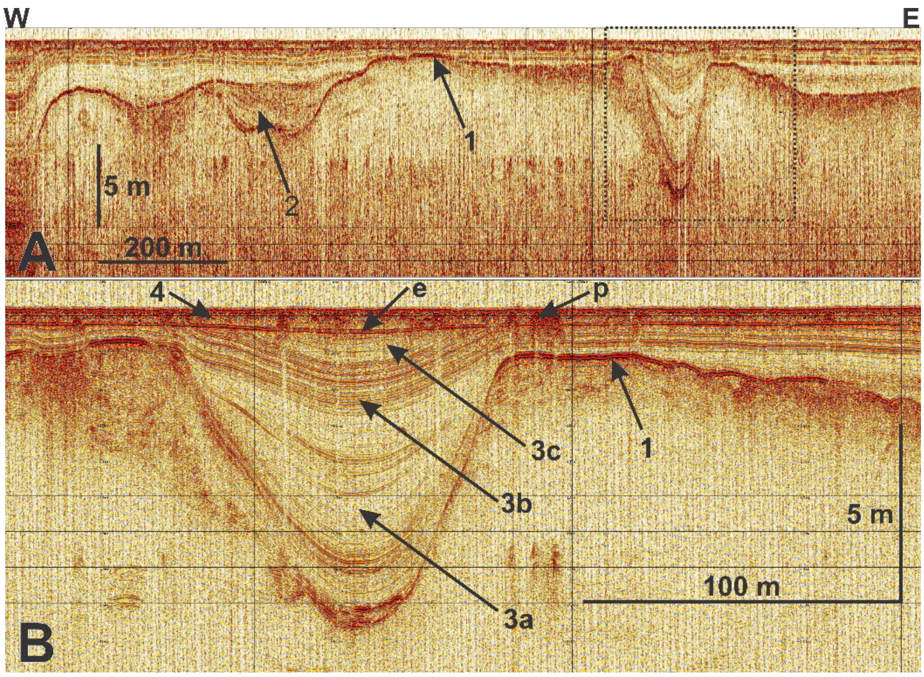

Figure 3: PES profile of W-E Line 2 at north of Tonlé Sap Lake (see L2 on Figure 1 for location), illustrating: A) several examples of palaeo-valleys, and B) detail of the infill of the palaeo-valley outlined in rectangle in A). PES Facies 1-4, labels and features are detailed in the text and Table 1.

3.2 Chronology and Sedimentation Rates

We used 11 new radiocarbon dates derived from the bulk sediment samples from our core LC2 to develop a bespoke age-depth model for that core (Figure 4a). In addition, our core and PES facies compare excellently, both with each other and with the previous studies of Day *et al*. (2011; Core TS-18-XII-03) and Fukumoto (2014; core CT10). The tight stratigraphic correlation between these cores, which can now confidently be made due to the availability of the PES data, thus makes it possible to undertake a meta-analysis of all the radiocarbon dates obtained from this study and the previously published core records. We thereby employed a total of 40 ^{14}C dates (Table 2) to create a new master chronology for the lake (Figure 4b). Consistent with prior studies, the age-depth models in both Figure 4a and Figure 4b reveal a distinct discontinuity in the rates of sedimentation above and below Facies 3 and 4. The sedimentation rates below 0.50 m (Facies 3) are relatively rapid, averaging *c*. 1.5 mm/year, as the basin accumulated *c*. 3.75 m sediment depth in just over 2,500 years (from 420 – 45 cm since *c*. 8,800 – 6,300 cal. yr BP). The onset of sedimentation above the discontinuity is somewhat older (*c*. 6.2k; Figure 4b) when compared to the value of between 4,450 and 3,910 cal. years BP estimated by Day *et al*. (2011), which could represent a N-S gradient of sedimentation rates. However, the key point is that the new PES data reveal that the discontinuity in fact represents an erosion surface, such that it is now clear that at least ~1.2 m of sediment accumulated in Facies 4 but was then lost due to widespread erosion. This missing sediment must have been eroded at some point in the interval between *c*. 6,200 - 2,000 cal. years BP. When accounting for this ~1.2 m of eroded sediment, the time-averaged sedimentation rate for Facies 4 decreases to *c*. 0.3 mm/year. Finally, it can be noted that dates gained within the top metre of sediments (Figure 4) show a consistent younging of dates upwards, suggesting that mixing within this layer has unlikely occurred to a major degree.

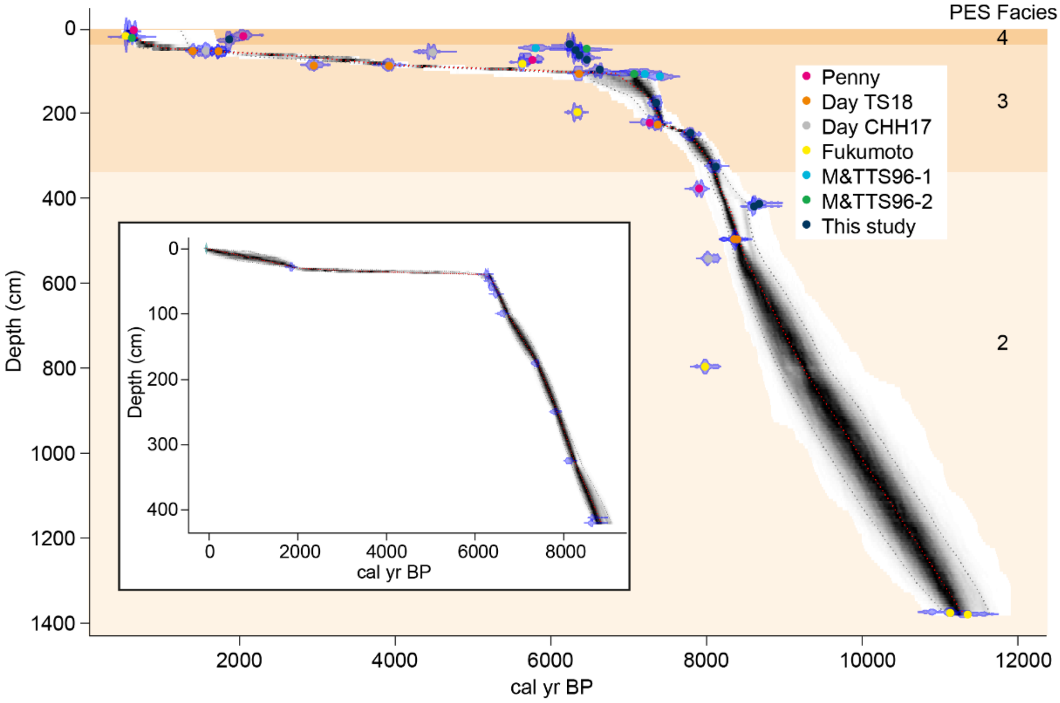

Figure 4. Age-depth model for the Tonlé Sap lake sediment sequences based on calibrated ^{14}C ages from (inset) the core sequence LC2 collected in this study and (main panel) a compilation of ^{14}C ages including those from sequence LC2 as well as prior studies (see Table 2). The calibrated ages were determined using the Calib 7.0 program and IntCal13 (Reimer *et al*., 2013). Note that the symbol shapes indicate the calibrated ^{14}C dates with two standard deviations, the grey shading indicates the likely age model and the dotted lines show the 95% confidence ranges of the age model. The age modelling was undertaken using the BACON package in R (Blaauw & Christen, 2011) with the following parameters: acc.mean=5; acc.shape=1.5; mem.mean=0.7; mem.strength=4. The boundaries between the different lithographic units (PES Facies 1 to 4) discussed in the text and Table 3 are also indicated.

3.3 Palaeo-environmental Reconstruction

The palaeo-environmental data show a number of marked changes throughout the core LC2 sequence (Figure 5), and we have chosen two elements from the Itrax data set to illustrate the key geochemical changes. The titanium plot (Figure 5) shows an oscillating, but long-term, decline from the earliest part of the sequence where organic sediments are preserved, around 420 cm, dated to *c*. 8,600 cal. yr BP, to around 120 cm (dated to *c*. 6,900 cal. yr BP). Titanium is often used as an inwash indicator, having a detrital origin, and as such can often be used to reflect relative changes in precipitation (e.g., Metcalfe *et al*., 2010; Swierczynski *et al*., 2012). The record shows enhanced Ti towards the base, with declining values thereafter, which could relate to a wetter early part of the record followed by relative drying. Nonetheless, the size of the basin and regional inflows means this could be an overly simplistic interpretation. The potassium record shows relatively little change throughout much of the record, but shows a marked change around 36 cm. Here we use K as a representative of the alkali/alkali earth elements that Day *et al*. (2011) used (Factor 2 elements, Fig 6), and our geochemical data are very similar to that from Day *et al*. (2011). This period in the sequence is difficult to date precisely, as the age/depth model suggests a coherent sequence exists until *c*. 36 cm (6,200 cal. yr BP), whereas by *c*. 30 cm, the sequence is dated to around 2,000 cal. yr BP. The change in K at around 36 cm is also reflected in a change in particle size and a relative decline in organic content from previously relatively high values. These changes are all indicative of a change in sediment coming into the lake at around 36 cm in the sequence.

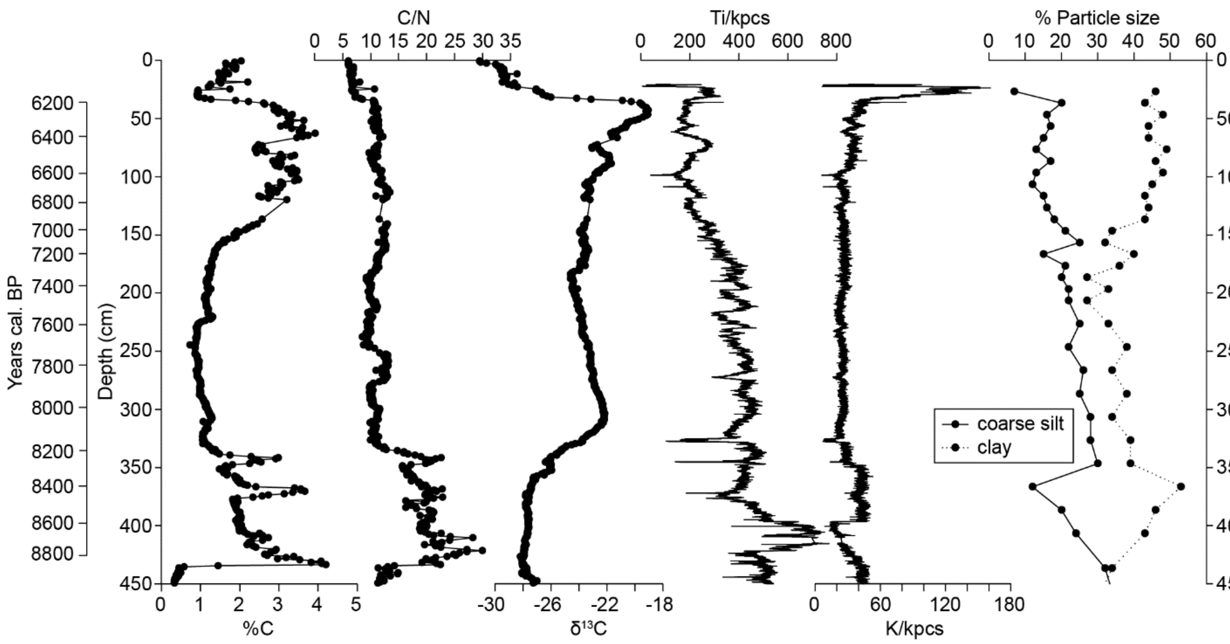

Figure 5. Palaeo-environmental proxies from the LC2 core taken in this study. Vertical axes show both depth, and calibrated ages (cal. yr BP) as calculated from our age model up to 36 cm depth (6,200 cal. yr BP). From left to right, the plots show %C, C/N ratios, $\delta^{13}C$, Itrax XRF Ti normalised against counts per second (kcps), Itrax XRF K normalised against counts per second, and percentage particle size for the coarse silt (62-31 microns) and clay (<3.9 microns) size fractions.

While the geochemical changes may reflect catchment precipitation and changes in sediment sources, organic matter (%C, C/N and $\delta^{13}C$) can indicate sediment sources, productivity, and whether the lake is a closed or open basin. The basal part of the sequence contains low %C, C/N and $\delta^{13}C$, most probably indicating an open freshwater system with the organic matter predominantly algal derived. From 430 to 330 cm (8,840-8,180 cal. yr BP), the C/N rises and is consistently >10, and mainly >20, and when coupled with low δ^{13}C (–28 to –25‰) suggests incorporation of terrestrial C3 plants from the catchment, which could relate to an expansion of C3 vegetation in the floodplain. There follows an interesting transition between 330 to 300 cm (8,180-8,010 cal. yr BP), where C/N falls, suggesting increased algal dominance, and increased δ^{13}C may reflect increased algal productivity, and the system remains relatively stable until 170 cm (7,250 cal. yr BP). After 170 cm, %C increases, C/N remains relatively low, indicative of an algal dominated system, and the high δ^{13}C is most likely aquatic productivity. The increase in %C, suggesting high productivity, coupled with a relative decline in Ti, may suggest a relatively drier system, perhaps moving towards a closed basin evaporative system. Above 50 cm (6,310 cal. yr BP), the low δ^{13}C and C/N are interpreted as a result of a change in algal communities but productivity is likely low, which, coupled with the geochemical data, may represent a change in sediment source.

3.4 Correlation of PES Facies with Core Records

The PES survey line that intersects our new core LC2 (Figure 6a) shows an excellent correspondence with the core description. The PES data (Figure 6a) show that the core was taken at the edge of a palaeo-valley, and displays the same four PES facies as summarised for the rest of the Tonlé Sap Lake (Table 1). It should be noted that core LC2 and the PES data were not taken at the same time (March 2013 and October 2014 respectively) and thus although the data match well, and geographic co-location is good, the resolution of the 2013 GPS data (*c.* 10-15 m) may result in a small error in their co-location. As shown by the PES data above, such small errors in co-location can potentially introduce some mismatch due to possible rapid changes in sediment thicknesses and facies types.

It is likely that our 4.58 m long core was unable to penetrate the hardened surface of the Pleistocene valley fill and thus this surface, and the sediments beneath (PES Facies 1) were not sampled. The basal 1.26 m of the core (458 to 332 cm) likely correlates to the lowest, rather structureless, PES reflections, which lay beneath the first very strong sets of reflections within the valley fill sediments at this locality. These lower sediments are interpreted to represent PES Facies 2 (fluvial or subaerial slope deposits) and indicate an open freshwater system with a large inwash of terrestrial C3 plants. Above this series of strong reflections, the next 3 m of sediment represents lacustrine sedimentation, with PES Facies 3 demonstrating a series of parallel reflections that drape the underlying topography. The lower part of this unit represents an algally-dominated freshwater lake (Facies 3a, b) but above *c.* 170 cm, and noticeably above the strong reflections that mark the base of PES Facies 3c (Figure 6a), the palaeo-environmental interpretation indicates a potentially drying climate and more evaporative lake conditions. The top *c*. 32 cm of Core LC2 correlates with PES Facies 4 and lies above the distinct erosion surface that can be correlated across the entire Tonlé Sap lake. These lacustrine sediments display a marked change in their geochemistry, and past work (Penny, 2006; Day *et al*., 2011; Fukumoto, 2014) shows a consensus that it is in these sediments, and during this time period, that the Mekong River became connected with the Tonlé Sap Lake. The characteristics of PES Facies 4 at the site of Core LC2 show feint parallel reflections and the presence of abundant point reflections, interpreted herein as being generated either by siderite concretions or shelly materials within this upper sediment.

The PES profile through the site of the Day *et al*. (2011) TS18-XII-03 core matches the corresponding core log very well (Figure 6b). Significantly, the distinct upper one metre (recall that this layer has isotopic signatures characteristic of sediments deposited within a flood-pulsing lake connected to the Mekong) corresponds closely to reflections that clearly delimit PES Facies 4 and which lie above the strong erosional base of this facies that can be traced across the entire lake. The section of the Day *et al*. (2011) TS18-XII-03 core below 1 m to 5 m depth appears linked to lacustrine PES Facies 3, with no evidence for Facies 2 at this site. The reflections here are rather weak, but parallel laminated sediment is clearly evident, terminating at 5 m depth against the strong reflection interpreted to represent the Pleistocene palaeo-valley surface of PES Facies 1. The core CT10 detailed by Fukumoto (2014) and a nearby PES section likewise match excellently despite being located approximately 1.3 km apart, but the PES provides a far higher level of resolution and lateral correlation. PES Facies 4 correlates well with Unit 7 of Fukumoto (2014), whilst the rather structureless Unit 6 of Fukumoto (2014), with weak reflections, matches PES Facies 3c. Unit 5 of Fukumoto (2014) shows a marked increase in the total diatom assemblage and it is noticeable how this correlates with a series of far stronger reflections in Facies 3b. Units 2, 3 and 4 of Fukumoto (2014) map onto Facies 3a, although it is noticeable that the core shows a region of higher diatom abundance within this region that again appears linked to a zone of stronger parallel reflections within Facies 3a. However, the spatial disparity between the CT10 core and PES panel do not allow closer correlation, and nor do the PES profiles here penetrate to the maximum depth of core CT10.

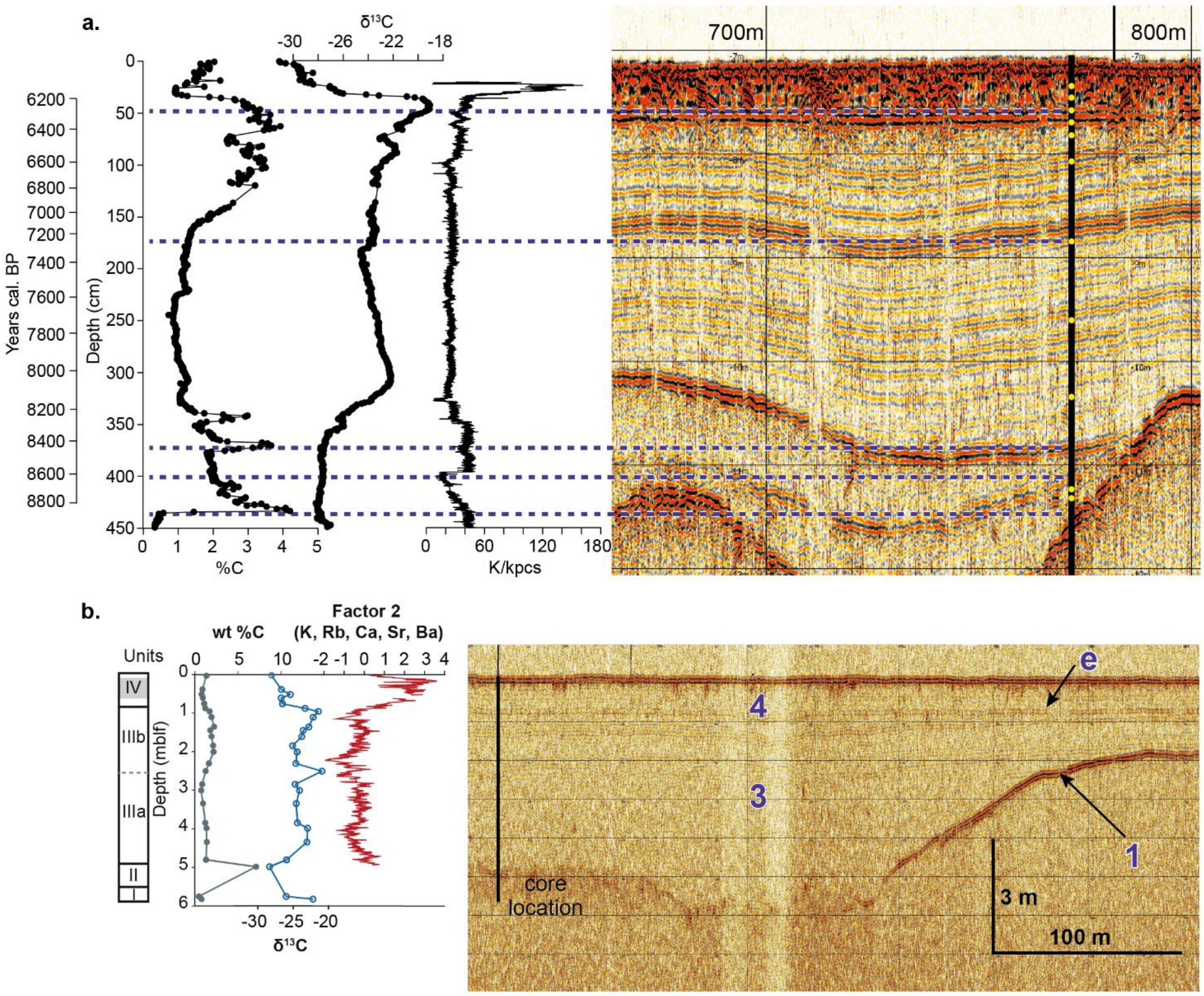

Figure 6. Examples of PES data showing the relationships between the Tonlé Sap Lake sediment PES facies determined from the geophysical surveys (right hand side) and selected palaeo-environmental datasets (left hand side). (a) Comparison of PES versus LC2 core (this study) data and (b) PES versus core from the study by Day (2011). Labels are detailed in the text and Table 1.

4. SYNTHESIS

The new data presented herein, together with the synthesis of previous research on the Tonlé Sap Lake and its Holocene history (Table 3), permit a unified synthesis of the palaeo-environmental changes that have led to its infill and changing rates of sedimentation. The background environmental and climate context to the development of the Tonlé Sap Lake, as inferred from a range of regional palaeo-records (Figure 7), is one of rapidly rising sea level of around 60 m from *c*. 11, 000 - 6,000 cal yr BP (Ta *et al*., 2002; Figure 7f). After the highstand of around 5 m above present day mean sea-level at *c*. 5,000 cal. yr BP, sea level starts to fall, through to the present day. During this period, the climate has oscillated considerably, and interpretation of the records is not straightforward. Yang *et al*. (2014) compare cave-based speleothem records from China (East Asian Summer Monsoon (EASM) region) with those from the Indian Summer Monsoon (ISM) region and argue that the coherence of the records, and modern source area of precipitation originating from the SW, implies the signature of these records is dominated by rainfall variability of the ISM region. Nonetheless, the trajectory of change is markedly similar, and likely implies a relatively stable (and likely wetter) early Holocene, with a clear change at around 6,000 cal. years BP to potentially drier conditions. Other records from the region, such as the Yulin loess-palaeosol record, show peaks in precipitation between *c*. 7,000 to 4,000 cal. yr BP, again with notable drying thereafter (Lu *et al*. 2013). This broad drying trend, from between *c*. 6,000 to 4,000 cal. yr BP, and into the later Holocene, can be compared with similar drying events identified from Lake Kumphawapi in Thailand (Figure 1) from between *c*. 6,500 to 1,400 cal. yr BP where multiple hiatuses are present, and that have been explained by periodic desiccation events of the wetland and erosion due to subsequent lake-level rise (Chawchai *et al*., 2015b; Figure 7c). The broad change in lake level, rising from *c*. 2,000 cal. yr BP, and reaching shallower parts around 1,400 cal. yr BP, is linked to a relative increase in effective precipitation, and compares well with a change in directional trend in the Chinese speleothem data, notably from Dongge Cave (Yang *et al*., 2014).

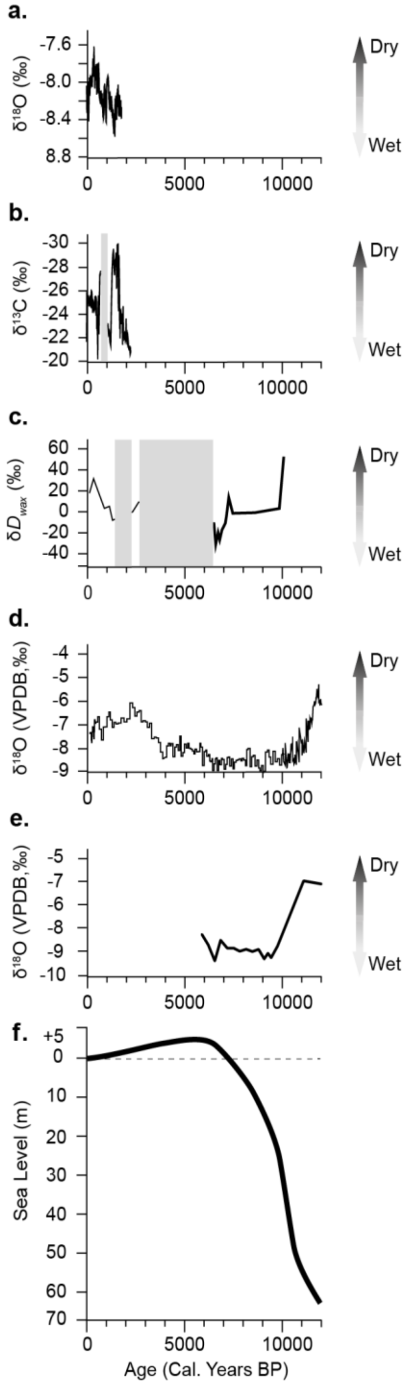

Figure 7. Synthesis of regional proxy records of climate change and sea-level rise from the present day to 15,000 cal. years BP based on: (a) $\delta^{18}O$ data from Wanxiang Cave (33°N, 105°E) speleothems (Zhang *et al*., 2008); (b) $\delta^{13}C$ data from the Lake Pa Kho (17°N, 102°E) sediment record (Chawchai *et al*., 2015a); (c) δD_{wax} (i.e., a hydrogen isotope proxy being the average value of C_{29} *n*-alkane and C_{31} *n*-alkane δD values)) data from the Lake Kumphawapi (17°N, 103°E) sediment record (Chawchai *et al*., 2015b); (d) $\delta^{18}O$ data from the Dongge Cave (25°N, 108°E) speleothem (Yuan *et al*., 2004); (e) $\delta^{18}O$ data from the Tham Lod and Ban Rai (19°N, 99°E) freshwater bivalve records (Marwick and Gagan, 2011), and; (f) Regional sea-level reconstruction for the Mekong delta region (Ta *et al*., 2002). Note that the grey shaded areas in panels (b) and (c) highlight areas with missing data due to an erosional hiatuses in the sediment records. The locations of the sites used in panels (a) through (e) are also illustrated on Figure 1.

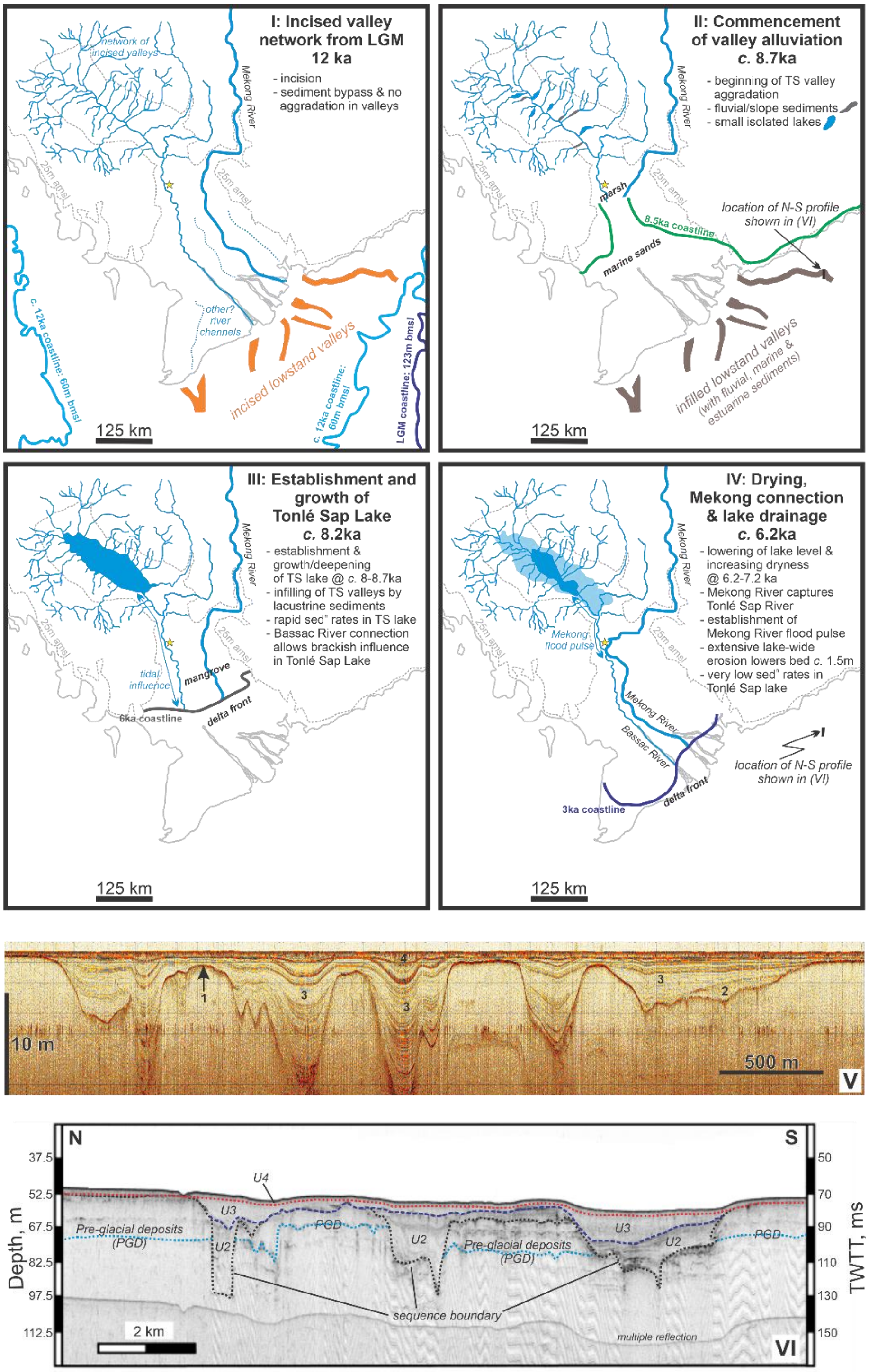

Figure 8. I-IV: Schematic palaeo-geographic reconstructions of the Holocene evolution of the Tonlé Sap Lake and Mekong delta. See text for explanation. Palaeo-shoreline positons and location of offshore incised palaeo-valleys after Nguyen *et al*. (2000), Tjallingii *et al*. (2010, 2014) and Zoccarato *et al*. (2018); V: Parametric Echo Sounder panel from the present study (this is part of L1 on Figure 1; see Figure 2 also for precise location), illustrating the palaeo-valleys and their infill. PES facies numbered as detailed in the text and Table 1; VI: Sub-bottom profile data from the Mekong coast (see location in Panel II) adapted from fig. 5 of Dung *et al*. (2013). See text for explanation. Sequence boundary is the LGM erosion surface and incised valleys. U2 and U3 are sediments that infill valleys and show the transition from fluvial to marine deposits. U2 is located at the base of the valley and represents possible fluvial lowstand to transgressive deposits. U3 is interpreted as transgressive estuarine to shallow marine deposits, whilst U4 is interpreted as a condensed section formed due to sediment starvation in the distal part of the highstand deposits (ages ranging from 0.3-8 ka).

The preceding synthesis presents an overall picture of rising and then falling (from *c*. 5,000 cal. yr BP) sea level, coupled with a mid-Holocene (*c.* 6,000 cal. yr BP) change in precipitation regime, that sets for the context for the Holocene evolution of the Tonlé Sap Lake through the stages that are described as follows and summarised in Figure 8:

1. Estimates of climate around the LGM in Southeast Asia are variable, but typically point to cooler temperatures (*e.g*., Zhang *et al*., 2019), with a reduced EASM, and precipitation from this period until *c.* 8ka may have been relatively reduced (Lu *et al*., 2013). Nevertheless, it is clear that erosion was taking place in the Tonlé Sap, creating a valley network that likely connected with the valleys that have also been detected and quantified (see Figure 8; Panel I) in the offshore surveys of Tjallingii *et al*. (2010, 2014), Dung *et al*. (2013) and Liu *et al.* (2017). In the Tonlé Sap region, the PES data reveal these valleys were a maximum of *c.* 15 m deep. These channels developed a complex network that likely fed into a main channel that flowed to the south (Figure 8; Panels I - V), perhaps connecting with the present day Bassac River and flowing to the present day coast, where subsurface data reveal Pleistocene valleys *c.* 20-30 m deep and defining a sequence boundary (Figure 8, Panel VI; Dung *et al*., 2013). These valleys thus fed sediment out to the Mekong delta through an incised lowstand valley network, with sediment bypass negating any significant valley aggradation. During this period, we speculate the principal Mekong River adopted a different course and thus had no influence on the Tonlé Sap River. Significant lowstand valleys detected in the present day coastal region (Figure 8; Panel I) bear witness to the multiple channels, or multiple positions of the main channel, through time.
2. Alluviation within the Pleistocene valley network of the Tonlé Sap region began at *c.* 8.7 ka at our core site (Figure 8; Panel II), as freshwater sediments with a high organic content and showing strong terrestrial characteristics, as evidenced through the C/N ratio and carbon isotopes data. We interpret our PES data as indicating fluvial or slope sedimentation, perhaps

with small isolated lakes in the valley network. This is supported by the interpretation of wetland environments during this time by Day *et al*. (2011). In the coastal region, Dung *et al*. (2013) interpret initial sedimentation as only occurring within the Pleistocene valleys, and as demonstrating an estuarine or fluvial nature (their Unit 2, Figure 8; Panel VI) as the valley network began to infill during sea-level rise. At this time, marine sands began to accumulate along a coastline where the Mekong delta was prograding to the south (Figure 8; Panel II).

3. Establishment of the Tonlé Sap Lake and major lacustrine sedimentation within these valleys (Figure 8; Panel III) began at *c*. 8.2 ka, and produced sedimentation that mantled the entire alluvial landscape, signifying growth and establishment of a lake that was eventually deep enough to drown the underlying topography. Flooding of the valley network, and establishment of the lake, must have occurred due to input from the river network, as well as possible incursions from the coast through the Bassac channel. This period marked the time of maximum sedimentation rates within the lake (*c*. 15 mm/year). Such lacustrine sedimentation characterises the majority of the infill of the valley network, with geochemical data indicating a likely climatic drying after *c.* 7,250 cal. yr BP, whose onset is shown by distinct strong reflections in the PES data, and also matches well with regional climate indices (Figure 7). Although our data do not reveal a marine or brackish water influence on sedimentation during deposition of Facies 3, Penny (2006) argued for a tidal and/or saline influence in the lake during the early to middle Holocene. We speculate that any connection of the Tonlé Sap Lake to the coast during this time was likely solely via the smaller Bassac River channel that would have permitted such a possibility, but without the need for a connection to the principal Mekong River. Saline intrusion, or backwater tidal effects, within the lake would be more likely in connections with a smaller channel, which would also not produce any change in sediment geochemistry as occurs after the connection to the Mekong River was established (see below). However, in the period after *c.* 7,250 cal. yr BP, the lake likely shrunk in volume and area due to this drying climate.

4. A period of widespread erosion occurred over the entire lake sometime after *c.* 6.2 ka (PES Facies 4) and produced the marked disconformity between PES Facies 3 and 4. This erosion event removed around *c.* 1.2 m of sediment across the entire lake, and sedimentation after this period was very different in both its much slower rate (*c.* 0.3 mm/year) and its marked compositional difference that shows a connection with the Mekong River (Table 3; Figure 8; Panel IV). Widespread erosion across the Tonlé Sap Lake was thus coincident with establishment of the flood pulse hydrology, generating the distinctive environment that is present today. We speculate this lake level lowering and erosion was linked to: (i) falling sea-level after the mid-Holocene highstand at *c.* 5,500 ka (Figure 7f) that would have increased river gradients; (ii) a period of enhanced climatic dryness that may also have lowered lake levels, potentially permitting enhanced wave erosion of the lakebed, and; (iii) avulsion of the Mekong River that allowed connection with the Tonlé Sap River and Lake, and potentially generated higher water surface slopes from the Tonlé Sap Lake during the dry season, as well as providing a larger conduit and water volume for the export of this sediment. From the depth of erosion of *c.* 1.2 m, and assuming a maximum lake area of 10,000 km^2, we estimate a volume of *c.* 12 km^3 of sediment was eroded during this period. The Mekong River delta was prograding to the south and by *c.* 3 ka had reached a location near its present-day position (Figure 8, Panel IV). Avulsion of alluvial channels is an omnipresent feature of deltas, and the Mekong River delta has undoubtedly experienced several such events in its Holocene advance. Although we have no data for the dating of such avulsions, topographic data for the current deltaic floodplain (Figure 9) reveal a series of abandoned channels, of approximately the same size as the present-day Mekong River, which likely bear witness to such events. We speculate herein that connection of the Mekong River to the Tonlé Sap drainage system, at some time after *c.* 6.2 ka, was through such an avulsion that enhanced and aided lake-wide erosion and export of this sediment to the delta.

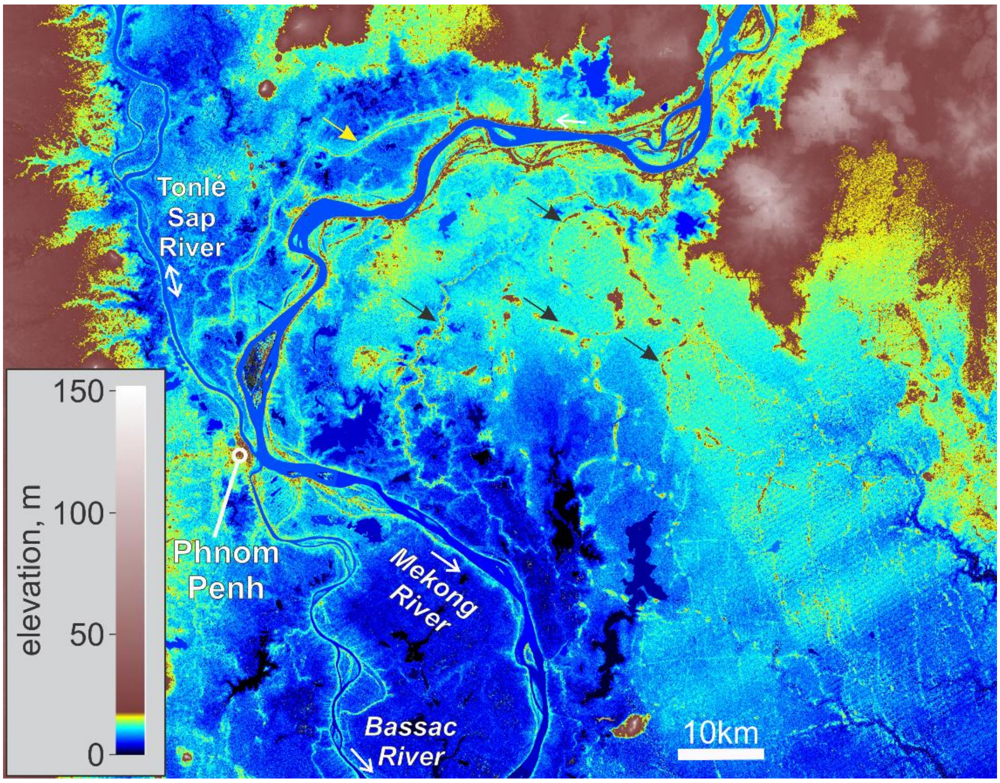

Figure 9. Topography of the Mekong River floodplain derived from SRTM data, illustrating the current Mekong, Bassac and Tonlé Sap rivers, together with the topographic signature of older palaeo-channels (labelled with black and yellow arrows) on the Mekong River floodplain. The sinuosity and width of these topographically elevated channels is of the same order as the current Mekong River, and may indicate the past positions of the Mekong main channel.

5. CONCLUSIONS

An annual flood pulse, whereby water from the Mekong River raises the lake level by *c*. 8m during the monsoon season, dominates the present-day hydrology of Cambodia's great lake, the Tonlé Sap. This flood-pulse is instrumental in bringing sediment and nutrients to the lake and its floodplain and provides a pathway for fish migration, establishing one of the richest fish habitats in Southeast Asia that is responsible for providing up to 80% of protein to Cambodia's growing population. In this study, we have presented new subsurface geophysical data, that when allied to new and past sediment core studies, unequivocally shows a period of major mid-Holocene erosion across the entire Tonlé Sap Lake that is coincident with establishment of the lake's critically important flood pulse. We argue that this widespread erosion, which removed at least 1 m of sediment across the entire lake, was triggered by base-level lowering due to capture of the Tonlé Sap drainage by the Mekong River, an event that would have significantly altered lake levels. This river capture also occurred during a period of falling sea-level after the mid-Holocene highstand, and after a period of climatic dryness, which would both have aided avulsion of the Mekong River and its capture of the Tonlé Sap River drainage network. Our new synthesis reconciles past anomalies in interpretation of Holocene palaeo-environmental change and sedimentation rates within the Tonlé Sap region, and demonstrates that interpretations of lacustrine sedimentation from cores must be set within the context of their broader spatial thickness changes as revealed by subsurface geophysical surveys. Establishing long-term sedimentation rates, or their fluctuation through time, cannot be assessed meaningfully without this broader context.

The present study demonstrates that longer-term landscape evolution of the Tonlé Sap region was thus punctuated by a rapid, river capture-induced, lake drainage that established the ecosystem that flourishes today. The scale of change induced by the capture illustrates the susceptibility of such systems to thresholds in geomorphic response, and highlights the perilous nature of ecosystem functioning in the Tonlé Sap to ongoing anthropogenic changes in hydrology and sediment flux within the Mekong River Basin.

Acknowledgements

This study was supported by a Gilchrist Educational Trust (in conjunction with the Royal Geographical Society with IBG) Fieldwork award, alongside awards NE/JO21970/1, NE/JO21571/1 and NE/JO21881/1 from the UK Natural Environmental Research Council (NERC). Funding from the Jack and Richard Threet Chair in Sedimentary Geology and Department of Geology, University of Illinois, allowed field travel for J.L.B and M.M. J.L.B. was in receipt of a University of Southampton Diamond Jubilee Fellowship that aided completion of this work.

Author Contributions

S.E.D, P.G.L, J.L., J.L.B, A.P.N, R.A and D.R.P jointly conceived the supporting grants; all authors co-designed the field investigations. P.G.L, J.L, S.E.D, M.J.L, S.B. and P.R.M collected and processed the sediment cores, while J.L.B, C.R.H and M.M. collected and processed the sub-bottom geophysical data. S.E.D, J.L.B, P.G.L and J.L jointly drafted the manuscript, which all authors then edited.

References

Ahmed, M., Hap, N., Ly, V. and Tiongco, M. (1998). Socioeconomic assessment of freshwater capture fisheries of Cambodia. A report on a household survey. MRC/DoF/Danida Project for the Management of the Freshwater Capture Fisheries of Cambodia. Mekong River Commission, Phnom Penh.

Arias, M. E., Cochrane, T. A., Piman, T., Kummu, M., Caruso, B. S. and Killeen, T. J. (2012). Quantifying changes in flooding and habitats in the Tonlé Sap Lake (Cambodia) caused by water infrastructure development and climate change in the Mekong Basin. Journal of Environmental Management, 112, 53–66.

Arias, M. E., Cochrane, T. A., Norton, D., Killeen, T. J. and Khon, P. (2013). The flood pulse as the underlying driver of vegetation in the largest wetland and fishery of the Mekong Basin. Ambio, 42, 864–876.

Arias, M. E., Cochrane, T. A., Kummu, M., Lauri, H., Holtgrieve, G., Koponen, J. and Piman, T. (2014). Impacts of hydropower and climate change on drivers of ecological productivity of Southeast Asia's most important wetland. Ecological Modelling, 272, 252–263.

Blaauw, M., Christen, J.A., 2011. Flexible paleoclimate age-depth models using an autoregressive gamma process. Bayesian Analysis, 6, 457-474

Carbonnel, J. P. and Guiscafré, J (1965). Grand Lac du Cambodge: Sedimentologie et hydrologie, 1962–1963. Muséum National d'Histoire Naturelle de Paris, Paris

Chawchai, S., Chabangborn, A. Fritz, S., Väliranta, M., Mörth, C-M., Blaauw, M., Reimer, P. J., Krusic, P. J., Löwemark, L. and Wohlfarth, B. (2015a). Hydroclimatic shifts in northeast Thailand during the last two millennia – the record of Lake Pa Kho. Quaternary Science Reviews, 111, 62-71.

Chawchai, S., Yamoah, K.A., Smittenberg, R. H., Kurkela, J., Väliranta, M., Chabangborn, A. Blaauw, M., Fritz, S. C., Reimer, P. J. and Wohlfarth, B. (2015b). Lake Kumphawapi revisited – The complex climatic and environmental record of a tropical wetland in NE Thailand. The Holocene, 26, 614-626; DOI: 10.1177/0959683615612565

Darby, S. E., Hackney, C. R., Leyland, J., Kummu, M., Lauri, H., Parsons, D., Best, J. L., Nicholas, A. P. and Aalto, R. (2016) Fluvial sediment supply to a mega-delta reduced by shifting tropical-cyclone activity. Nature, 539, 276-279; doi:10.1038/nature19809.

Day, M. B., Hodell, D. A., Brenner, M., Curtis, J. H., Kamenov, G. D., Guilderson, T. P., Peterson, L. C., Kenney, W. F. and Kolata, A. L. (2011). Middle to late Holocene initiation of the annual flood pulse in Tonlé Sap Lake, Cambodia. Journal of Paleolimnology, 45, 85-99; doi: 10.1007/s10933-010-9482-9

Dung, B.V., Stattegger, K., Unverricht, D., Van Phach, P. and Thanh, N.T. (2013) Late Pleistocene-Holocene seismic stratigraphy of the Southeast Vietnam shelf, Global and Planetary Change, 110, 156-169.

Fukomoto, Y. Holocene climate changes in East Asia reconstructed from boring sediments in lakes and peatlands, PhD Thesis, Kyushu University, Japan (2014).

Fuji, H., Garsdal, H., Ward, P., Ishii, M., Morishita, K. and Boivin, T. (2003). Hydrological roles of the Cambodian floodplain of the Mekong River. International Journal of River Basin Management, 1, 1–14.

Hortle, K. G. Consumption and the yield of fish and other aquatic animals from the Lower Mekong Basin. Mekong River Commission Technical Paper No. 16, Mekong River Commission, Vientiane (2007).

Hung, N. N., Delgado, J. M., Tri, V. K., Hung, L. M., Merz, B., Bárdossy, A. and Apel, H. (2012). Floodplain hydrology of the Mekong Delta, Vietnam. Hydrological Processes, 26, 674-686; doi: 10.1002/hyp.8183

International Center for Environmental Management (ICEM). Strategic Environmental Assessment on the Mekong Mainstream. Summary of the Final Report. Prepared for the Mekong River Commission by International Center for Environmental Management. (2010).

Innomar (2016) *SES-2000 Users Guide ISE 2.9.5 Post Processing Software*, 198 pp.

Inomata, H. and Fukami, K. (2008). Restoration of historical hydrological data of Tonlé Sap Lake and its surrounding areas. Hydrological Processes, 22, 1337–1350.

Junk, W. J., Bayley, P. B. and Sparks, R. E. (1989). The flood pulse concept in river-floodplain systems". In *Proceedings of the International Large River Symposium (LARS), Canadian Special Publication of Fisheries and Aquatic Sciences* Edited by: Dodge, D. P. Vol. 106, 110–127.

Junk, W. J. (1997a). General aspects of floodplain ecology with special reference to Amazonian floodplains. In *The Central Amazon Floodplain. Ecology of a Pulsing System*, Edited by: Junk, W. J. 3–20. Berlin Heidelberg: Springer-Verlag. Ecological Studies 126

Junk, W. J. (1997b). Structure and function of the large Central Amazonian River floodplains: synthesis and discussion. In *The Central Amazon Floodplain. Ecology of a Pulsing System*, Edited by: Junk, W. J. 455–472. Berlin Heidelberg: Springer-Verlag. Ecological Studies 126

Junk, W., Brown, M., Campbell, I., Finlayson, M., Gopal, B., Ramberg, L., Warner, B. (2006). The comparative biodiversity of seven globally important wetlands: a synthesis. Aquatic Sciences - Research Across Boundaries, 68, 400–414.

Kite, G. (2001). Modelling the Mekong: hydrological simulation for environmental impact studies. Journal of Hydrology, 253, 1-13; doi: 10.1016/S0022-1694(01)00396-1

Kummu, M., Tes, S., Yin, S., Adamson, P., Józsa, J., Koponen, J., Richey, J. and Sarkkula, J. (2014) Water balance analysis for the Tonlé Sap Lake–floodplain system. Hydrological Processes, 28, 1722–1733; DOI:10.1002/hyp.9718

Kummu, M., Lu, X. X., Wang, J. J. and Varis, O. (2010). Basin-wide sediment trapping efficiency of emerging reservoirs along the Mekong. Geomorphology, 119, 181–197.

Kummu, M. and Sarkkula, J. (2008). Impact of the Mekong river flow alteration on the Tonlé Sap flood pulse. Ambio, 37, 185–192.

Lamberts, D. (2006). The Tonlé Sap Lake as a productive ecosystem. International Journal of Water Resources Development, 22:3, 481-495; DOI: 10.1080/07900620500482592

Lamberts, D. (2008). Little impact, much damage: the consequences of Mekong River flow alterations for the Tonlé Sap ecosystem. In *Modern Myths of the Mekong - A Critical Review of Water and Development Concepts, Principles and Policies*, Kummu, M., Keskinen, M. and Varis, O. (eds). Water and Development Publications, Helsinki University of Technology, Finland; 3–18.

Lamberts, D. and Koponen, J. (2008). Flood pulse alterations and productivity of the Tonlé Sap ecosystem: a model for impact assessment. Ambio, 37, 178–184.

Liu, J.P., DeMaster, D.J., Nittrouer, C.A., Eidam, E.F. and Nguyen, T.T. (2017) A seismic study of the Mekong subaqueous delta: Proximal versus distal sediment accumulation, Cont. Shelf Res., 147, 197-212.

Lu, H. et al. (2013). Variation of East Asian monsoon precipitation during the past 21 k.y. and potential CO_2 forcing. Geology, 41, 1023-1026.

Marwick, B. and Gagan, M.K. (2011). Late Pleistocene monsoon variability in northwest Thailand: an oxygen isotope sequence from the bivalve Margaritanopsis laosensis excavated in Mae Hong Son province. Quaternary Science Reviews, 30, 3088-3098.

Mekong River Commission (MRC). Overview of the Hydrology of the Mekong River Basin, Mekong River Commission. Vientiane, Laos (2005).

Mekong River Commission (MRC). Toward Better Investments in Water Resource Management and Development, Mekong River Commission. Vientiane, Laos (2018).

Metcalfe, S. E., Jones, M. D., Davies, S. J., Noren, A. and MacKenzie, A. (2010). Climate variability over the last two millennia in the North American monsoon region, recorded in laminated lake sediments from Laguna de Juanacatlán, Mexico. The Holocene, 20, 1195-1206; doi: 10.1177/0959683610371994

Mildenhall, D. C. (1996). Report on two pollen samples from Lake Tonlé Sap, Cambodia. Institute of Geological and Nuclear Sciences, New Zealand.

Nguyen, V.L., Ta, T.K.O. and Tateishi, M. (2000) Late Holocene depositional environments and coastal evolution of the Mekong River Delta, Southern Vietnam, J. Asian Earth Sciences., 18, 4270439.

Okawara, M. and Tsukawaki, S. (2002). Composition and provenance of clay minerals in the northern part of Lake Tonlé Sap, Cambodia. Journal of Geography (Chigaku Zasshi), 111, 341–359.

Penny, D. (2006). The Holocene history and development of the Tonlé Sap, Cambodia. Quaternary Science Reviews, 25, 310-322; doi: 10.1016/j.quascirev.2005.03.012

Piman, T., Lennaerts, T. and Southalack, P. (2013). Assessment of hydrological changes in the lower Mekong basin from basin-wide development scenarios. Hydrological Processes, 27, 2115-2125; doi: 10.1002/hyp.9764

Pottier, C., Penny, D., Hendrickson, M. and Carter, E. A. (2012). Unearthing an Atlantean myth in Angkor: geoarchaeological investigation of the ‘underwater road’ crossing the Tonlé Sap Lake, Cambodia. Journal of Archaeological Science, 39, 2604-2611; doi:10.1016/j.jas.2012.04.005

Rainboth, W. J. FAO Species Identification Field Guide for Fishery Purposes. Fishes of the Cambodian Mekong, FAO, Rome (2006).

Reimer, P. J., Baird, E., Bayliss, A. et al. (2013). INTCAL13 and MARINE13 Radiocarbon age calibration curves 0-50,000 years cal BP. Radiocarbon, 55, 1869-1887.

Sambrook Smith, G. H., Best, J. L., Orfeo, O., Vardy, M. E. and Zinger, J. A. (2013). Decimeter-scale in situ mapping of modern cross-bedded dune deposits using parametric echo sounding (PES): a new method for linking river processes and their deposits, Geophysical Research Letter., 40, 3883-3887; doi: 10.1002/grl.50703.

Sambrook Smith, G. H., Best, J. L., Leroy, J. Z. and Orfeo, O. (2016). The alluvial architecture of a suspended sediment dominated meandering river: the Rio Bermejo, Argentina, Sedimentology, 63, 1187–1208; doi:10.1111/sed.12256.

Sverdrup-Jensen, S. (2002). Fisheries in the Lower Mekong Basin: Status and Perspectives, Mekong River Commission Technical Paper No. 6, Mekong River Commission, Phnom Penh

Swierczynski, T., Lauterbach, S., Dulski, P., Delgado, J., Merz, B. and Brauer, A. (2012). Mid- to late Holocene flood frequency changes in the northeastern Alps recorded in varved sediments of Lake Mondsee (Upper Austria). Quaternary Science Reviews, 80, 78-90; doi: 10.1016/j.quarscirev.2013.08.018

Ta, T.K.O., et al. (2002). Holocene delta evolution and sediment discharge of the Mekong River, southern Vietnam. Quaternary Science Reviews, 21, 1807–1819.

Tjallingii, R., Stattegger, K., Wetzel, A. and Phac, P. V. (2010). Infilling and flooding of the Mekong River incised valley during deglacial sea-level rise. Quaternary Science Reviews, 29, 1432-1444; doi: 10.1016/j.quascirev.2010.02.022

Tjallingii, R., Stattegger, K., Stocchi, P., Saito, Y. and Wetzel, A. (2014) Rapid flooding of the southern Vietnam shelf during the early to mid-Holocene, J. Quaternary Sci., 29, 581-588.

Tsukawaki, S. Okuno, M. and Nakamura, T. (1997). Sedimentation rates in the northern part of Lake Tonlé Sap, Cambodia, during the last 6,000 years. *Sam. Res. Using AMS at Nagoya Univ., Dat. Mater. Res. Center, Nagoya Univ*., 8, 125-133.

Yang, X., Liu, J., Liang, F., Yuan, D., Yang, Y., Lu, Y. and Chen, F. (2014). Holocene stalagmite $\delta^{18}O$ records in the East Asian monsoon region and their correlation with those in the Indian monsoon region. The Holocene, 24, 1657-664.

Yuan, D., Cheng, H., Edwards, R.L., Dykoski, C.A., Kelly, M.J., Zhang, M., Qing, J., Lin, Y., Wang, Y., Wu, J., Dorale, J.A., An, Z. and Cai, Y. (2004). Timing, duration, and transitions of the last interglacial Asian monsoon. Science, 304, 575-578.

Zhang, E., Chang, J., Shulmeister, J., Langdon, P.G., Sun, W., Cao, Y., Yang, X., Shen, J. (2019). Summer temperature fluctuations in SW China during the end of the LGM and the last deglaciation. *Earth and Planetary Science Letters*, 509, 78-87.

Zhang, P., et al. (2008). A test of climate, Sun and culture relationships from an 1810-year Chinese cave record, Science, 322, 940–942, doi:10.1126/science.1163965.

Ziv, G., Baran, E., Nam, S., Rodriguez-Iturbe, I. and Levin, S. A. (2012). Trading-off fish biodiversity, food security, and hydropower in the Mekong River Basin. Proceedings of the North American Academy of Sciences, 109, 5609-5614; doi: 10.1073/pnas.1201423109

Zoccarato, C., Minderhoud, P.S.J. and Teatini, P. (2018) The role of sedimentation and natural compaction in a prograding delta: insights from the mega Mekong delta, Vietnam, Scientific Reports, 8, DOI:10.1038/s41598-018-29734-7.

Table 1. Description and Interpretation of PES Facies Characteristics

PES Facies	Reflector Characteristics	Interpretation
1	Marked by a strong upper reflection than most often has no, or very faint, reflections beneath (Fig. 2 inset; labelled 'a'). Where present, most of these underlying reflectors are non-parallel and discontinuous and cannot be traced over distances greater than *c.* 100m. The strong upper reflection horizon may be very close to, or at, the present-day lake surface (Figs 2 and 3; labelled 1), but is often markedly erosional with a relief of up to *c.* 15m, with broad depressions that may be up to *c.* 1.2km in width (Fig. 2) but are frequently 50-200m wide (Fig. 2). This strong reflection is present within the vast majority of PES lines over the entire lake.	Eroded surface of a buried Pleistocene valley network
2	Lies directly above Facies 1, and consists of either structureless, or faintly bedded, sediments that are either non-parallel or downlap onto, and truncate against, the lower basal reflection (Figs 2 and 3, labelled '2'). Some of these surfaces and inclined, and define accretion onto the underlying basal erosion surface and lateral to the underlying valley margins (Fig. 2; labelled '2'). Facies 2 is up to 2 m thick but occurs in only a few of the PES survey lines.	Fluvial, or subaerial slope deposits. Initial stages of Pleistocene valley infill.
3	Dominant PES facies within the Tonlé Sap Lake in terms of thickness and volume of deposits, and consists of strong reflections that are largely parallel, and sub-parallel, to eachother and the underlying reflections, and drape the underlying topography (Figs 2 and 3, labelled '3'). These reflections sometimes drape the entire topography of Facies 1, but may also taper out laterally (Fig. 2; labelled 'l'). Facies 3 does not possess any clear internal cross-cutting relationships between reflections, but a range of different strength reflections can be used to subdivide the facies into three subunits (Fig. 3), although all these reflections are conformable and drape the underlying topography. The lower reflections (Facies 3a; Fig. 3) consist of rather weak parallel beds, with several stronger reflections within the middle of this package. Facies 3a ranges from *c.* 0.5 to 6m thick. Facies 3b conformably overlies Facies 3a (Fig. 3) but is noticeable for possessing a series of much stronger reflections, that in total may be up to 2 m in thickness. Lastly, Facies 3c possesses a series of more diffuse and weaker reflections (Fig. 3), but that are still parallel bedded, drape the underlying sediments conformably and may be up to 1.5m thick. Facies 3 shows a wide variation in thickness, from a maximum of *c.* 10 m to a minimum of zero where the present day lake surface intersects the strong reflections of Facies 1.	Lacustrine sedimentation with conformable deposition of sediment from suspension. Some of the lower drapes mantle the entire topography at the valley edges (Figs 2 & 3) and demonstrate that the lake was deep enough to drown the palaeo-valley landscape and was established by the commencement of Facies 3 deposition.
4	Facies 4 lies uncomfortably on Facies 3 and is *c.* 0.7-1m thick over much of the northern and southern parts of the lake (Figs 2 and 3). Characterised by very strong flat, parallel, reflections that are laterally extensive, and the basal reflector of this facies is often very strong (Figs 2 and 3, labelled 'e') and notably has a markedly erosive contact with the underlying Facies 3 (Fig. 2 inset p x). This unit is characterised by frequent parabolic reflections that may occur singly or in clusters (Fig. 2, inset, labelled 'p'), and when in groups these parabolic reflections may lessen the strength of the underlying reflections, highlighting their probable high density in attenuating acoustic penetration. The nature of the unconformable lower contact may show a very marked angular divergence with the underlying sediments (Fig. 2, inset panel x, dashed line). If the thickness of the parallel reflectors that are truncated is examined, this indicates erosion of *c.* 1.2m of sediment (Fig. 2, inset panel x) during this erosive event. However, the amplitude of relief along this erosional surface is small, with one N-S transect line in the north of the Tonlé Sap Lake (labelled line 'L' on Fig. 1) showing an erosional relief of 0.95m along a transect length of *c.* 28 km.	Sedimentation in Tonlé Sap lake due to sediment suspension settling, but after a period of widespread erosion that generated the extensive erosion surface that separates Facies 3 and 4 across all of the Tonlé Sap lake. Parabolic point reflections generated from diagenetic siderite concretions (Pottier *et al.*, 2012), or accumulations of the clam *Corbicula fluminaea* (Penny, 2006) within the sediments.

Table 2. Synthesis of ^{14}C dates for Tonlé Sap lake core records. Core depth (in cm) is given below the sediment-water interface adjusted to a common datum. See Figure 1 for the locations of each core. Calibration of the ^{14}C dates was made using Calib 7.0 and IntCal13 (Reimer *et al*., 2013). Age ranges shown are the highest relative probability for the calibrated ^{14}C dates.

Lab ID	Core depth (cm)	^{14}C BP ± 1σ	Material	Calibrated age range (2σ)	Source
Beta-463010	28.5	1910 ± 30	Plant material	1857 ± 94	This study
Beta-463011	39.5	5450 ± 30	Bulk sediment	6247 ± 48	This study
Beta-463012	49.5	5520 ± 30	Bulk sediment	6312 ± 59	This study
Beta-463013	59.5	5610 ± 30	Bulk sediment	6375 ± 68	This study
Beta-444816	69.5	5680 ± 30	Bulk sediment	6459 ± 68	This study
Beta-444817	99.5	5810 ± 30	Bulk sediment	6616 ± 106	This study
Beta-444818	175.5	6420 ± 30	Bulk sediment	7360 ± 71	This study
Beta-444819	249.5	6960 ± 30	Bulk sediment	7790 ± 111	This study
OxA-28154	324.5	7308 ± 30	Wood	8107 ± 74	This study
OxA-28155	411.5	7864 ± 33	Wood	8641 ± 106	This study
OxA-28156	419.5	7834 ± 33	Wood	8610 ± 80	This study
AA-39964	7	650 ± 35	Pollen grains	603 ± 59	Penny (2006)
CAM-66653	16	2070 ± 40	Pollen grains	2040 ± 105	Penny (2006)
CAM-66654	72	4990 ± 40	Pollen grains	5717 ± 139	Penny (2006)
AA-39963	221	6345 ± 45	Pollen grains	7280 ± 122	Penny (2006)
CAM-66655	378	7090 ± 40	Pollen grains	7923 ± 78	Penny (2006)
CAMS-137174	53	1530 ± 35	Shell	1425 ± 87	Day *et al*. (2011)*
CAMS-137172	54	1800 ± 30	Shell	1732 ± 98	Day *et al*. (2011)*
CAMS-137173	55	1800 ± 30	Shell	1732 ± 98	Day *et al*. (2011)*
CAMS-121346	86	2845 ± 35	Wood	2954 ± 98	Day *et al*. (2011)*
CAMS-138882	86	3605 ± 35	Bulk sediment	3914 ± 117	Day *et al*. (2011)*
CAMS-140615	106	5580 ± 40	Bulk sediment	6360 ± 70	Day *et al*. (2011)*
CAMS-140616	223	6465 ± 40	Bulk sediment	7373 ± 75	Day *et al*. (2011)*
CAMS-138883	497	7545 ± 40	Bulk sediment	8369 ± 101	Day *et al*. (2011)*
CAMS-121347	497	7570 ± 60	Wood	8381 ± 155	Day *et al*. (2011)*
SUERC-29792	52	1663 ± 37	Bulk sediment	1568 ± 138	Day *et al*. (2011)$^{+}$
SUERC-29793	55	3978 ± 36	Bulk sediment	4462 ± 115	Day *et al*. (2011)$^{+}$
SUERC-29794	542	7228 ± 40	Bulk sediment	8040 ± 95	Day *et al*. (2011)$^{+}$
POZ-45741	16	535 ± 30	Shell	543 ± 60	Fukomoto (2014)
POZ-45742	80	4910 ± 40	Bulk sediment	5637 ± 65	Fukomoto (2014)
POZ-45743	198	5530 ± 40	Bulk sediment	6332 ± 62	Fukomoto (2014)
POZ-45745	797	7180 ± 50	Bulk sediment	7995 ± 139	Fukomoto (2014)
POZ-37573	1375	9680 ± 50	Wood	11110 ± 213	Fukomoto (2014)
POZ-37574	1380	9950 ± 50	Plant charcoal	11373 ± 186	Fukomoto (2014)
Not reported	46	5081 ± 86	Bulk sediment	5816 ± 189	Mildenhall (1996)
Not reported	102	6233 ± 84	Bulk sediment	7133 ± 206	Mildenhall (1996)
Not reported	114	6505 ± 88	Bulk sediment	7415 ± 149	Mildenhall (1996)
Not reported	20	620 ± 100	Mollusc shell	605 ± 130	Tsukawaki *et al.* (1997)
Not reported	50	5620 ± 120	Bulk sediment	6421 ± 266	Tsukawaki *et al.* (1997)
Not reported	106	6070 ± 90	Bulk sediment	6939 ± 239	Tsukawaki *et al.* (1997)

Notes: Dates from This Study, Penny (2006), Fukomoto (2014), Mildenhall (1996) and Tsukawaki *et al* (1997) are for ^{14}C samples taken from Cores LC2, S2C1, CT10, TS96-1 and TS96-2, respectively. For the ^{14}C dates from Day *et al*. (2011), the symbol * indicates dates taken from core TS-18-XII-03 whereas + indicates dates taken from core CHH-17-XII-03.

Table 3. Characteristics of the PES Facies compared with palaeo-environmental data from this and other studies.

PES Facies	PES Interpretation	LC2 core interpretation (this study)	Day (2011): 2 cores, both have 4 distinct units	Fukumoto (2014)	Penny (2006)
1	Eroded surface of a buried Pleistocene valley network				Not present
2	Fluvial, or subaerial slope deposits. Initial stages of Pleistocene valley infill.	457-434cm (older than 8760 cal. yr BP). Low %C, C/N and $\delta^{13}C$. A freshwater open system with low productivity. 434-332cm (>8760 – 8190 cal. yr BP). Relatively high but variable %C, C/N, and initially high Ti. High precipitation with large inwash of terrestrial C3 plants.	Unit 1 (older than 8380 cal yr BP). Low %C, C/N. Interpreted as wetland/lacustrine. Unit 2 (age centred on 8380 cal yr BP). Increase %C and C/N. Very depleted $\delta^{13}C$. Wetland interpretation.	Zone 1 and part zone 2? (from 12.3k cal yr. BP). Development of lake, with some evidence of marsh. End of zone 2 (ends 8000 cal. yr BP). Diatoms indicate possible increased production between 8400-8000 cal. yr BP.	Likely not present
3	Lacustrine sedimentation with conformable deposition of sediment from suspension. Some of lower drapes mantle the entire topography at the valley edges (Figs 2 & 3) and demonstrate that the lake was deep enough to drown the palaeo-valley landscape and was established by the commencement of Facies 3 deposition.	332-32cm (8190-6170 cal. yr BP). Low %C, C/N, and enriched $\delta^{13}C$, with declining Ti and stable particle size. Likely increased production, algal dominated freshwater lake system. From 170cm onwards (7250 cal. yr BP) production increases, which may be linked to a drying climate (reduced Ti), with finer grain size and more closed evaporative system. 7250 cal. yr BP is seen as a clear reflector in PES.	Unit 3. (age *c.* 8300-6360 cal yr BP). Initial phase of low %C but increasing after c. 7370 cal. yr BP. Interpreted as shallow non-pulsing lake, with greater detrital input pre *c.* 7370 cal. yr BP, and diminished detrital input thereafter.	Zones 3-5 (8000-6400 cal. yr BP). Low %C and diatoms indicate a strongly turbid lake, possibly enhanced in size early in the zone (wetter). Clear change at 7300 cal. yr BP, after which lake levels may be lower and finer grain size input.	Zones 1 and 2 (from *c.* 8000 cal. yr BP. Unclear end of zone, but pre-5890 cal. yr BP). Argues for some marine influence and mangrove pollen possibly being local. There is no clear indication of a reflector around 7300 cal. yr BP, but zone change in vegetation occurs *c.* 6500 cal yr. BP.
4	Sedimentation in Tonlé Sap lake due to sediment suspension settling, but after a period of widespread erosion that generated the extensive erosion surface that separates PES Facies 3 and 4 across all of the Tonlé Sap lake. Parabolic point reflections generated from diagenetic siderite concretions~~, of siderite and manganese~~ (Pottier *et al.*, 2012)~~,~~; or accumulations of the clam *Corbicula fluminaea* (Penny, 2006) within the sediments.	32-0cm. (age uncertain due to erosive events below this unit). Large changes in organics and large increases in K suggests an erosive surface, with an algal dominated lake. Lower relative production as indicated by the lower %C and relatively depleted $\delta^{13}C$. Flood-pulsing lake connected to the Mekong River.	Unit 4 (age relatively uncertain, but estimate to begin between c. 4,450 and 3,910 cal. year BP). Large change into this unit indicated by altered Sr and Nd isotopes, and broad changes in geochemistry. Interpreted as now flood-pulsing lake, connected to Mekong River.	Zones 6 and 7 (post 6400 cal yr BP). Complete change in diatom flora. Lower lake levels and increased bottom water anoxia.	Zone 2 and 3. The major change in sedimentological data, coupled with a change in vegetation (relative increase in *Macaranga*) occurs around 100cm. Difficult to date but the signature compares clearly with a shift from Facies 3 to 4.